Interface fracture property of PEO ceramic coatings on aluminum alloy

YongJun Guan [a,b], Yuan Xia [a,*], FangTao Xu [a]

[a] Institute of Mechanics, Chinese Academy of Sciences, Beijing 100190, China
[b] State Key Laboratory of Automotive Safety and Energy, Department of Automotive Engineering, Tsinghua University, Beijing 100084, China

Abstract

This paper combines the four-point bending test, SEM and finite element method to study the interface fracture property of PEO coatings on aluminum alloy. The interface failure mode of the coating on the compression side is revealed. The ceramic coating crack firstly along the 45° to the interface, then the micro crack in the coating deduces the interface crack. The plastic deformation observed by SEM shows excellent adhesion property between the coating and substrate. The plastic deformation in the substrate is due to the interfacial crack extension, so the interface crack mode of PEO coatings is ductile crack. The results of FEM show that the compression strength is about 600 MPa.
© 2008 Elsevier B.V. All rights reserved.

Keywords: PEO coatings; Interface fracture; Four-point bending; Finite element method

1. Introduction

Plasma electrolytic oxidation (PEO) coatings are gaining more and more attention[1]. Combining electrochemistry oxidation with plasma discharge in electrolyte, PEO technique produces ceramic coatings with excellent properties such as high hardness [2–5], wear resistance [6–10], corrosion resistance [11–16] and thermal protection [17,18]. The thickness of PEO coating can be easily controlled, to the maximum of around 200 μm, by adjusting process parameters. Because of all the advantages mentioned above, PEO technique is very promising for a number of industrial applications.

Because of partial consumption of the substrate during the process, PEO coatings should have high resistance to interfacial spallation due to strong bonding at the interface. According to Nie [6], the thin inner layer of the coatings near the interface exhibits a number of sublayers, and the lower portion of the intermediate layer has a nanoscaled polycrystalline microstruc-ture. Gnedenkov [19] used pull tests and scratch tests to study adhesion property of PEO coatings on aluminum alloy. Their results show that the adhesion strength exceeds 82 MPa, which is the adhesive glue tension strength. Despite some early reports about the adhesion of PEO coatings, the interface fracture property of PEO coatings needs further studies.

The present study focuses on the failure analysis of PEO coating deposited on aluminum alloy substrates using four-point bending. The work reveals the mechanism of cohesive cracking and spallation in the coating by cross-sectional SEM analysis. In addition, finite element method is adopted to simulate the deformation and stress in the coating/substrate system.

2. Research routine and experimental details

PEO experimental equipment is shown in Refs. [20,21]. Al–Cu–Mg 2024 aluminum alloy plate was used as the substrate material, and aqueous solution of sodium silicate with concentration of 20 g/L was used as the electrolyte. The coated plate is cut into beams with the size of 50 mm in length, 8 mm in width and 1 mm in height. The as-deposited coatings were polished with SiC paper to remove the outer loose layer. Polished PEO coating exists only on the top side of the beam, with a thickness of about 150 μm.

* Corresponding author. Institute of Mechanics, Chinese Academy of Sciences No.15 Beisihuanxi Road, Beijing, China, 100190. Tel./fax: +86 10 82543858.
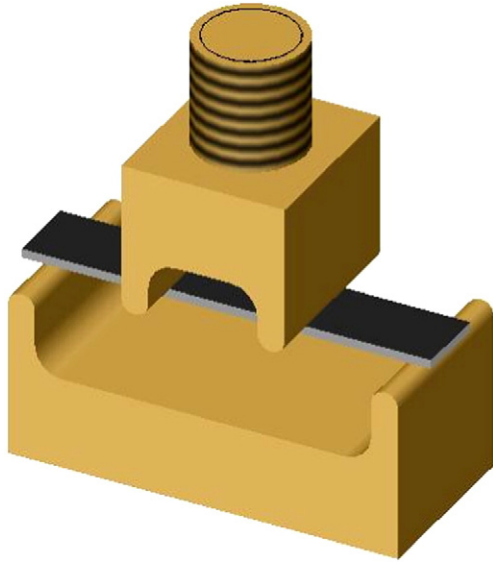   *E-mail addresses:* gyj@tsinghua.edu.cn (Y.J. Guan), xia@imech.ac.cn (Y. Xia).

Fig. 1. Sketch map of four-point bending test.

The schematic illustration of test equipment is shown in Fig. 1. During the four-point bending test, PEO coating is in compression stress state to prevent vertical crack in the coating. The distance between the outer pins is 40 mm; the distance between the inner pins is 15 mm. The specimen was loaded in displacement control mode with a constant loading velocity. Load and displacement history is recorded by the micro computer system. The sudden drop in the load curve is used to characterize the initial failure of the coating.

After the failure, SEM is used to study the cross section and interface profiles. The interface crack is so long that the whole interface profile cannot be contained in one SEM picture. Therefore, many SEM pictures are combined to give the whole profile. After the PEO coating is stripped off the substrate, the morphologies of both sides near the interface are characterized by SEM. The element composition of delaminated surfaces of substrate and PEO coating is characterized by EDS.

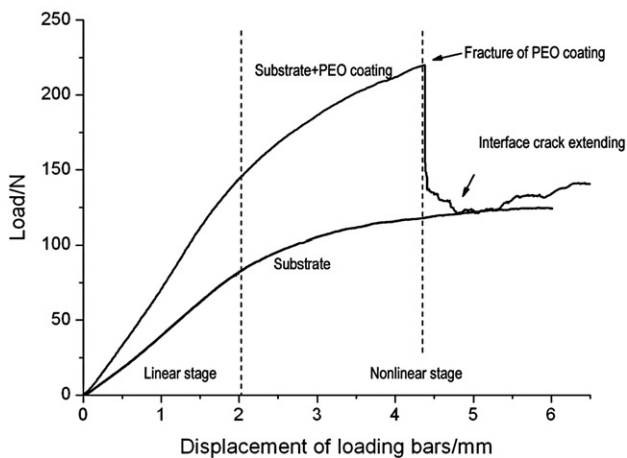In the finite element model, substrate is considered as linear strain-hardening elastic-plastic material with elastic module of 73 GPa, yielding stress of 274 MPa and strain-hardening modulus of 1.46 GPa. The local elastic module of PEO coating gained by nano-indentation is 210 GPa. However, according to Ref. [17], the global modulus of PEO coating is less than the local modulus gained by nano-indentation, and the global modulus gained by bi-material beam cooling experiments is about 40 GPa. So in the finite element model, PEO coating is considered as elastic material with elastic modulus of 40 GPa. Interface between coating and substrate is considered as perfect adhesion. The FE model is loaded at the critical level according
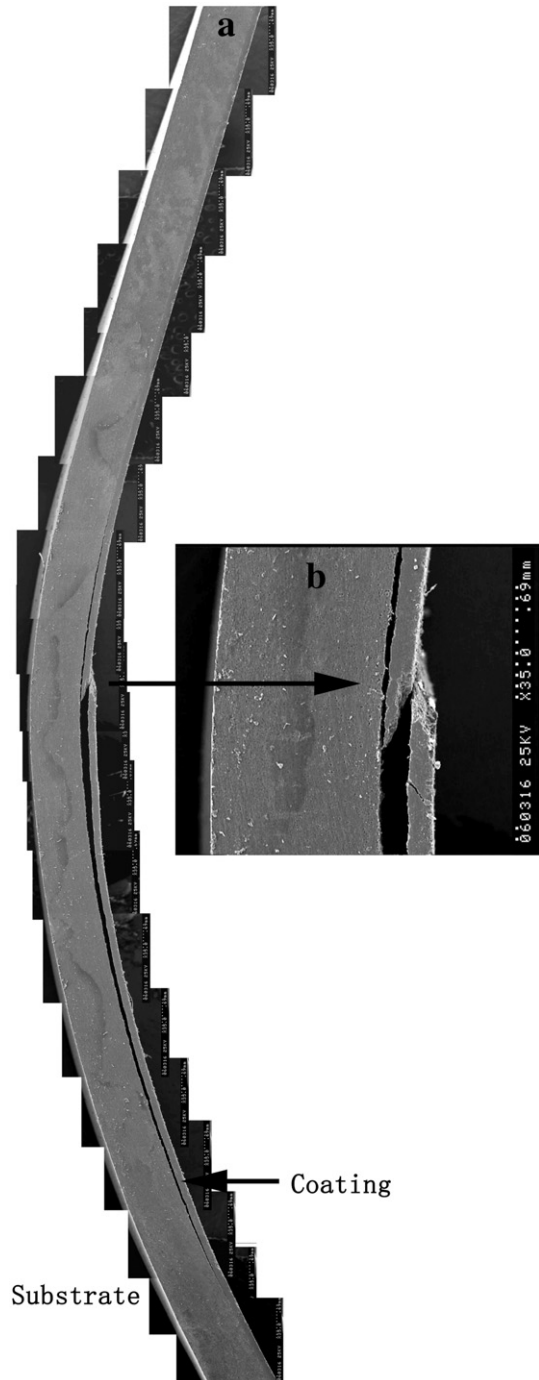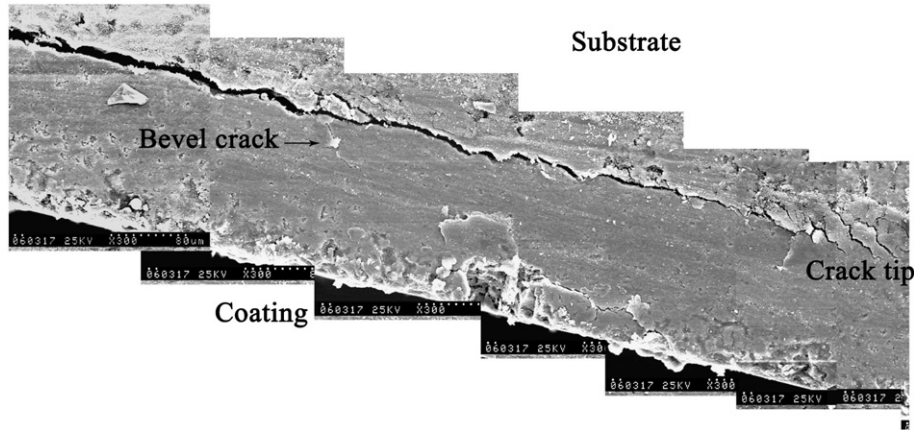

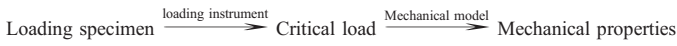Fig. 3. Interface fracture of PEO coating.

Fig. 2. Load–displacement curves of four-point bending.

Fig. 4. Interface crack tip of PEO coating.

to the test results. The routine adopted in this paper can be demonstrated as shown below.

$$\text{Loading specimen} \xrightarrow{\text{loading instrument}} \text{Critical load} \xrightarrow{\text{Mechanical model}} \text{Mechanical properties}$$

3. Experimental results and discussion

Fig. 2 gives the load–displacement curves for PEO coated specimen and uncoated specimen. The loading process of the coated specimen can be divided into three stages: linear stage, nonlinear stage and failure stage. In the initial loading stage, both the loads increase proportionally to displacement while the stiffness of PEO coated beam is much larger than that of uncoated specimen. PEO coating on the compression side increased the antibending ability of the specimen significantly. Under the

condition of this paper, the coated specimen bears twice the load of uncoated specimen at the same displacement. Following the initial linear stage, nonlinear stage commences which is due to plastic deformation and geometric nonlinearity. In nonlinear stage, the loads required to continue the deformation increase with the increase of displacement. Following the nonlinear stage, the loading curve for PEO coated specimen has a sudden drop at a critical load level, which can be explained by the failure of the coating. After the critical failure point, the loading curve is changed from smooth mode to rough mode, which corresponding to the extending of interfacial crack. The interface crack extends with the increasing displacement until the maximum displacement is reached.

The cross-sectional microphotographs after failure are shown in Fig. 3. Before the failure initiates, the coating bears mainly compression stress, and the 45° section is the maximum
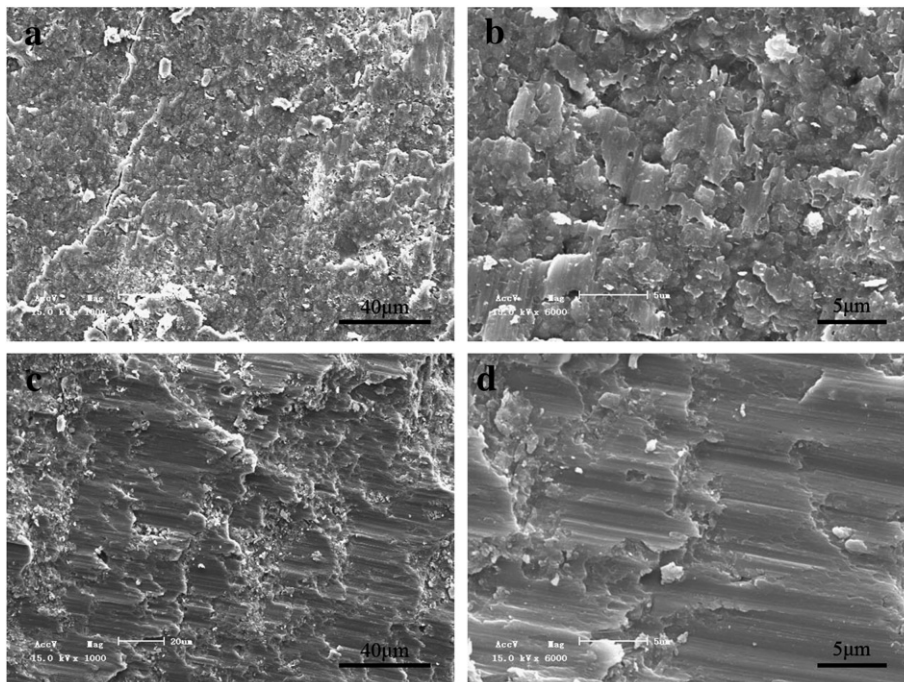

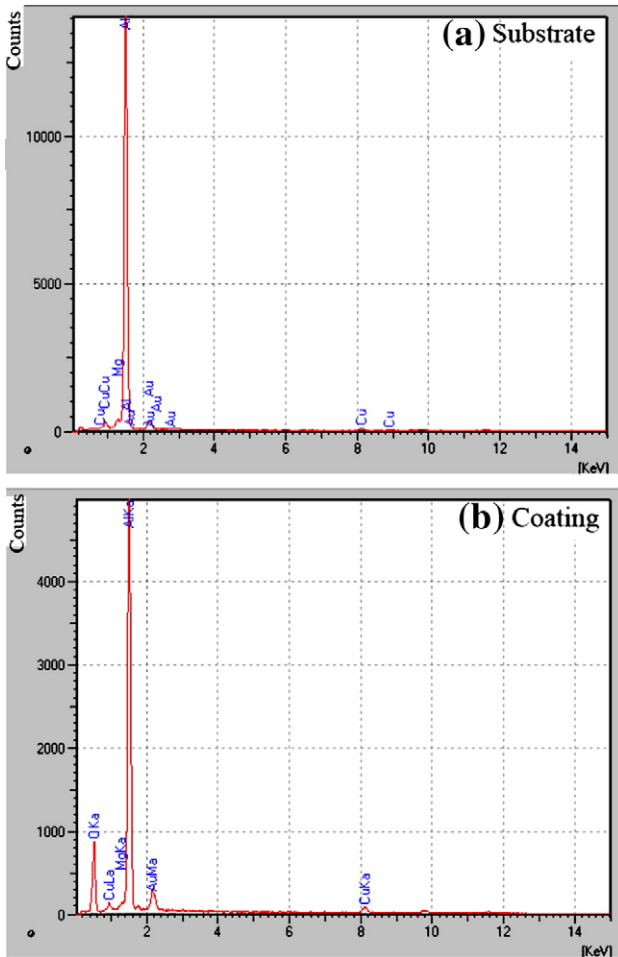Fig. 5. Interface morphologies after delamination a,b) coating c,d) substrate.

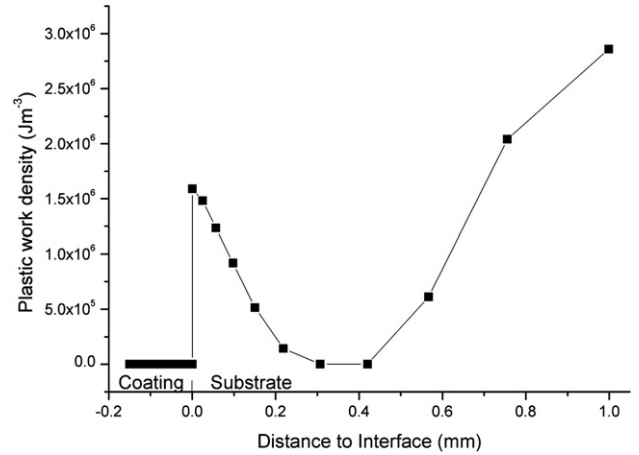Fig. 6. EDS result of delaminate surface a) substrate b) PEO coating.

Fig. 8. Distribution of plastic work density along the thickness on symmetry side.

crack tip. Micro cracks with 45° to the interface exist near the crack tip. In the same figure, bevel cracks also exist in the delaminated coating. So a conclusion can be drawn that during the failure process, the interface crack is induced by the micro cracks with 45°.

Fig. 5 shows the microphotographs of the fracture surface after delamination. During the PEO process, part of the substrate is oxidized and sintered into ceramic coating. Sintered particles can be seen in Fig. 5a and b. After delamination of PEO coating, obvious plastic deformation appears in the aluminum alloy substrate near the interface. As is well known, a ductile crack absorbs more energy during crack extension. The plastic deformation near the interface shows that the interface crack of PEO coating is ductile crack.

Fig. 6 shows the EDS results of delaminated surfaces of substrate (Fig. 6a) and PEO coating (Fig. 6b). The EDS result from the substrate contains mainly Al and alloy elements indicating Fig. 5c and d is a clean metal surface instead of an inner layer of coating. The EDS result PEO coating contains O, Al and alloy elements of substrate. According to the EDS results

shear stress section in the coating. When the critical load is reached, shear failure takes place. This failure mode is consistent with the failure mode of typical brittle material under compression load. After the failure initiates, crack propagates along the interface. Fig. 4 shows morphology of the interfacial
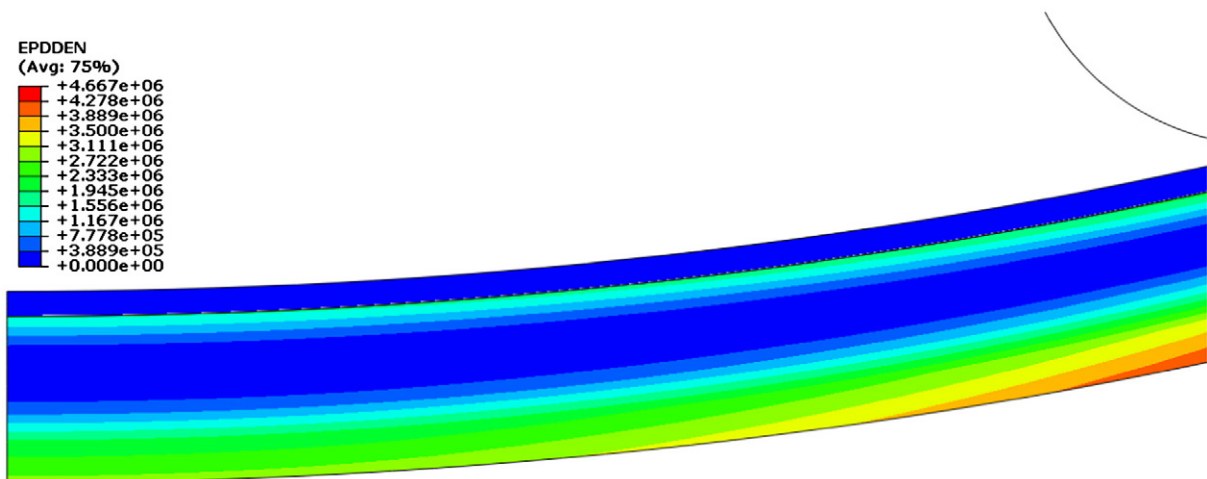

Fig. 7. Contour of plastic work density at critical load.

of delaminated surfaces of substrate and PEO coating, a conclusion can be drawn that the failure is truly interfacial.

4. Finite element simulation results

Fig. 7 shows the distribution of plastic work density at the critical load but before failure. It is very clear that the plastic deformation exists in the tension part and interface of the specimen. Plastic work near the interface indicates the plastic deformation before delamination, which shows a ductile fracture of interface. The plastic work distribution on the symmetric section is shown in Fig. 8, which also demonstrates this point.

Fig. 9 demonstrates the stress distribution along the thickness direction on the symmetric section. Normal stress component parallel to the beam length direction (SX) is compression stress near the surface of the coating with a value about 556 MPa. The compression stress decreases with the increasing depth and drop to 406 MPa near the interface. Because of the elastic module mismatch between the coating and substrate, compression stress has a sudden change across the interface. The compression stress in the substrate near the interface is about 283 MPa, which is higher than the yielding stress of aluminum alloy. Normal stress component perpendicular to the beam length direction (SY) and the shear stress (SXY) are so low that can be neglected comparing with normal stress parallel to the beam length direction (SX). The stress state in the coating can be regarded as pure compression stress state with the value of SX. The maximum SX before the failure can be used to characterize the compression strength of the PEO ceramic coatings.

Fig. 10 shows the distribution of the compression stress on the surface of the coating along the length of the beam specimen. The local stress concentration is due to the loading bars. Combining the distribution of principal compression stress along the length and the tested initial position of the failure, the compression strength of PEO coatings is about 600 MPa.

5. Conclusion

In this paper, the interface fracture property of PEO coating on aluminum alloy is studied using a four-point bending test.
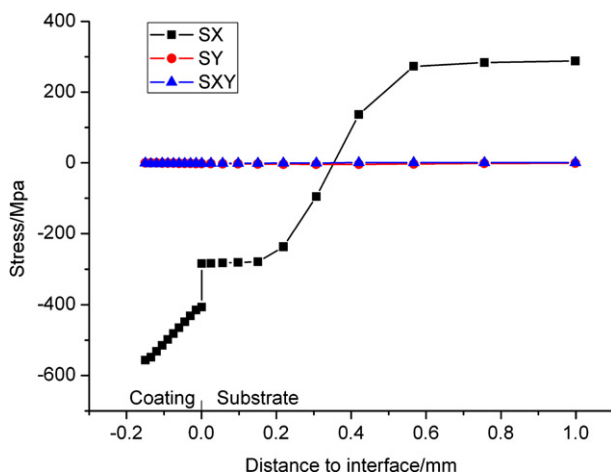
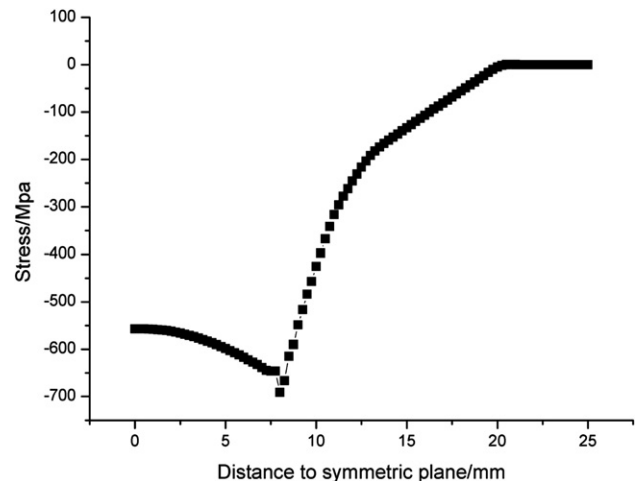Fig. 9. Stress distribution along the cross section.

Fig. 10. Surface compression stress distribution along the length.

By putting PEO coating on the compression side, the interfacial failure of PEO coating is revealed. First, the ceramic coating fracture on the 45° section because of the maximum shear stress. Then micro bevel cracks in the coating induce the onset and extension of interfacial crack. Plastic deformation near the interface shows that the interface crack of PEO coating is ductile crack. Combining test results and FE simulation, the compression strength of PEO coatings is determined to about 600 MPa.

References

[1] A.L. Yerokhin, X. Nie, A. Leyland, A. Matthews, S.J. Dowey, Surf. Coat. Technol. 122 (2–3) (1999) 73.
[2] X. Nie, A. Leyland, H.W. Song, A.L. Yerokhin, S.J. Dowey, A. Matthews, Surf. Coat. Technol. 119 (1999) 1055.
[3] L.R. Krishna, K.R.C. Somaraju, G. Sundararajan, Surf. Coat. Technol. 163 (2003) 484.
[4] H.H. Wu, H.B. Wang, B.Y. Long, B.H. Long, Z.S. Jin, N.D. Wang, F.G. Yu, D.M. Bi, Appl. Surf. Sci. 252 (5) (2005) 1545.
[5] W.B. Xue, C. Wang, Z.W. Deng, R.Y. Chen, Y.L. Li, T.H. Zhang, J. Phys.-Condens. Matter 14 (44) (2002) 10947.
[6] X. Nie, E.I. Meletis, J.C. Jiang, A. Leyland, A.L. Yerokhin, A. Matthews, Surf. Coat. Technol. 149 (2–3) (2002) 245.
[7] J. Tian, Z.Z. Luo, S.K. Qi, X.J. Sun, Surf. Coat. Technol. 154 (1) (2002) 1.
[8] T.B. Wei, F.Y. Yan, J. Tian, J. Alloy. Compd. 389 (1–2) (2005) 169.
[9] L.R. Krishna, A.S. Purnima, G. Sundararajan, Wear 261 (10) (2006) 1095.
[10] X. Nie, L. Wang, E. Konca, A.T. Alpas, Surf. Coat. Technol. 188–89 (2004) 207.
[11] W.B. Xue, X.L. Wu, X.J. Li, H. Tian, J. Alloy. Compd. 425 (1–2) (2006) 302.
[12] Z.P. Yao, Z.H. Jiang, X.H. Wu, X.T. Sun, Z.D. Wu, Surf. Coat. Technol. 200 (7) (2005) 2445.
[13] Y. Ma, X. Nie, D.O. Northwood, H. Hu, Thin Solid Films 494 (1–2) (2006) 296.
[14] H.P. Duan, K.Q. Du, C.W. Yan, F.H. Wang, Electrochimica Acta 51 (14) (2006) 2898.

[15] R.C. Barik, J.A. Wharton, R.J.K. Wood, K.R. Stokes, R.L. Jones, Surf. Coat. Technol. 199 (2–3) (2005) 158.

[16] J. Liang, B.G. Guo, J. Tian, H.W. Liu, J.F. Zhou, W.M. Liu, T. Xu, Surf. Coat. Technol. 199 (2–3) (2005) 121.

[17] J.A. Curran, T.W. Clyne, Surf. Coat. Technol. 199 (2–3) (2005) 168.

[18] J.A. Curran, T.W. Clyne, Surf. Coat. Technol. 199 (2–3) (2005) 177.

[19] S.V. Gnedenkov, O.A. Khrisanfova, A.G. Zavidnaya, S.L. Sinebrukhov, P.S. Gordienko, S. Iwatsubo, A. Matsui, Surf. Coat. Technol. 145 (1–3) (2001) 146.

[20] Y.J. Guan, Y. Xia, Trans. Nonferr. Met. Soc. China 15 (3) (2005) 565.

[21] Y.J. Guan, Y. Xia, Trans. Nonferr. Met. Soc. China 16 (5) (2006) 1097.